Annals of Glaciology 17 1993

The response of lead patterns in the Beaufort Sea to storm-scale wind forcing

BERNARD A. WALTER
SAIC, 13400 B Northup Way, Suite 36, Bellevue, WA 98005, U.S.A.

JAMES E. OVERLAND
NOAA/PMEL, 7600 Sand Point Way NE, Seattle, WA 98115, U.S.A.

ABSTRACT. With the use of time series of AVHRR imagery we examine a non-typical case of ice motion and lead pattern formation in the Beaufort Sea during a period of persistent southwesterly to southerly winds during 31 March–14 April 1991. Our goal is to suggest sea-ice rheologies through the use of satellite imagery. Ice motions were estimated by making a negative of the first image in a time sequence and combining it with a second image using a logical AND operation. Thus leads for the first day are white and those for the second day are black. For the period 31 March–5 April with westerly winds there was a slip line oriented southwest–northeast across the central Beaufort Sea and another slip line parallel to it 150 km to the north. Relative motion was 0.015 m s^{-1} across the slip lines. With southerly winds during 9–14 April the entire field of leads was advected to the north. Lead patterns are organized on a hierarchy of scales and the scales are a result of the particular magnitude of forcing by the atmosphere. Angles between diamond-shaped lead features with spacings of both 150 km and 10–20 km are approximately 30°, which as Erlingsson showed corresponds to an angle of internal friction of 15°. We provide an argument for the scale-invariant nature of the lead patterns and suggest that it may be possible to parameterize small-scale (less than tens of km) lead patterns.

INTRODUCTION

The routine availability of imagery from polar orbiting meteorological satellites over Arctic sea ice made possible the first large-scale studies of the patterns of open water or leads and thin ice. Studies have focused on the geometrical shapes of the patterns, their lengths and widths, their formation and disappearance, and ultimately the identification of specific mechanisms of lead formation.

Researchers have investigated the formation of and changes to lead patterns on a variety of spatial and temporal scales. Marko and Thomson (1977) focused on the large scale (hundreds of km) rectilinear or diamond-shaped patterns formed by networks of intersecting leads in the ice and concluded that these features were a result of semi-brittle failure of the ice cover during relatively rapid strain rates due to wind forcing. Sobczak (1977) mapped the distribution of leads and basin-scale ice movement over the Beaufort Sea and found that the passing of atmospheric pressure systems developed various sea-ice patterns which depended on the rate of movement of the systems and the intensity of the pressure gradients. Recently Barry and others (1989) found that in some cases lead orientations could change noticeably within 24 h while in other cases the leads exhibited substantial persistence of orientation. They show that periods of persistence occurred when ice concentration was high and ice velocities low, suggesting the influence of internal ice stresses. Steffen (1987) noted that the distribution of fractures in ice is a measure of the capacity of the ice cover to sustain deformation through convergence and shear. Thus one might expect that quantitative measurements of lead pattern changes might provide information about the stress state and mechanical properties of the ice (Erlingsson, 1988, 1989, 1991; Pritchard, 1988).

We present results from a case study of lead pattern change and movement in the Beaufort Sea during a period of southwesterly to southerly winds. A time series of AVHRR images during 31 March to 14 April 1991 was combined with digitized sea-level pressure fields to determine the influence that the wind forcing had on the lead patterns. This was during the period of the LEADEX pilot experiment. Changes in the lead patterns are seen as a horizontal movement of the leads or as the appearance or disappearance of certain geometric lead configurations such as the large diamond-shaped patterns. These larger-scale diamond-shaped lead patterns were seen to maintain their shapes and spacings for periods of three to four weeks. We describe the meteorological conditions present during the study period, and relate the meteorological forcing to the behavior of the lead patterns. We note that the atmospheric forcing changes direction and magnitude on scales of days to a week. Finally, we discuss the presence of smaller-scale lead patterns within the larger

https://doi.org/10.3189/S0260305500012878 Published online by Cambridge University Press

diamond-shaped patterns and the implications of this phenomenon to the scale invariant nature of the features seen in ice fields.

LEAD PATTERN CHANGES

Digital AVHRR imagery were collected once and sometimes twice per day over the Beaufort Sea (most often at 1300–1400 h GMT). The images were navigated and remapped to a common grid. Sea-level pressure analyses were obtained every 6 h from the Anchorage Weather Service Forecast Office to track the movement of significant weather features such as fronts. Digitized sea-level pressure fields obtained from the National Meteorological Center were used to calculate surface wind fields using a 30% reduction in speed and a 20° rotation in direction. The wind fields were then remapped to the same grid as the satellite images.

From satellite imagery the Beaufort Sea could be divided spatially into two distinct lead pattern regimes. These regimes were initially separated by a long lead running diagonally from southwest to northeast across the Beaufort Sea (Fig. 1). This lead appeared to be the result of a persistent southwesterly flow over the Beaufort Sea which compacted the ice located south of this line against the eastern boundary of the Beaufort Sea, formed by Banks, Melville and the Queen Elizabeth Islands, but allowed ice motion on the north side of this lead.

North of the diagonal lead the dominant lead configuration was the diamond-shaped pattern discussed by Marco and Thomson (1977). These large curvilinear and rectilinear lead patterns (Erlingsson, 1991) with spacings in the order of 150 km were formed by two intersecting sets of leads. In general, acute angles of intersection were in the range 20–40°. Within the large-scale (150 km) diamond-shaped patterns there were also smaller-scale (10 s km) diamond-shaped features whose directions were similar to the orientations of the larger-scale lead pattern. South of the diagonal lead the large-scale lead patterns were curved and oriented in a north–south direction apparently due to the no-slip boundary between the coastline and the open ice pack.

The period can be divided into several wind-forcing regimes. Prior to 7 April the time series of surface geostrophic winds showed that winds were nearly parallel to the long diagonal lead (Fig. 2). A weak frontal system moved across the Beaufort on 5 April with winds behind

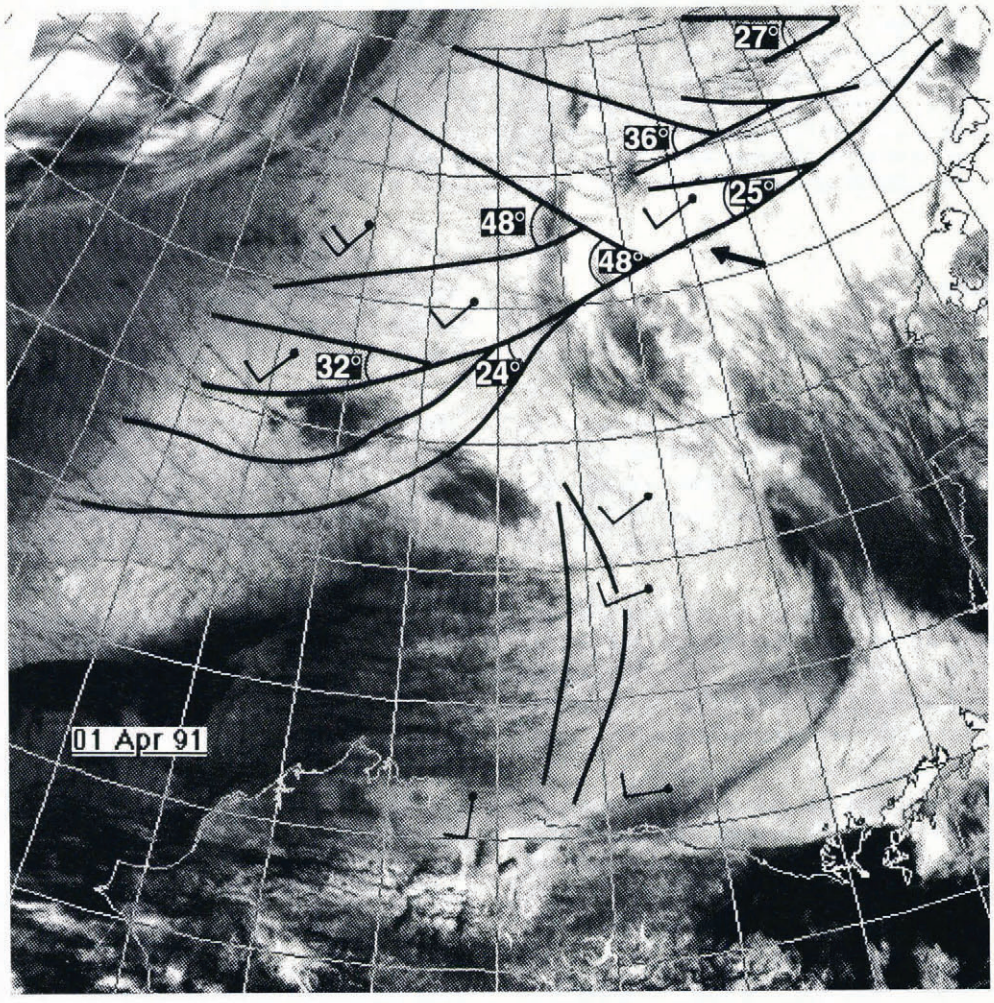

Fig. 1. AVHRR image (3 km resolution) for 1300 h GMT, 1 April 1991. The image shows a long lead (arrow) running diagonally southwest to northeast across the Beaufort Sea with large-scale diamond-shaped lead structures north of this line and arch-shaped lead structures running basically northward from the coast and merging with the diamond-shaped features to the north. Surface winds (in kt) are also plotted on the image using the standard meteorological convention.

https://doi.org/10.3189/S0260305500012878 Published online by Cambridge University Press

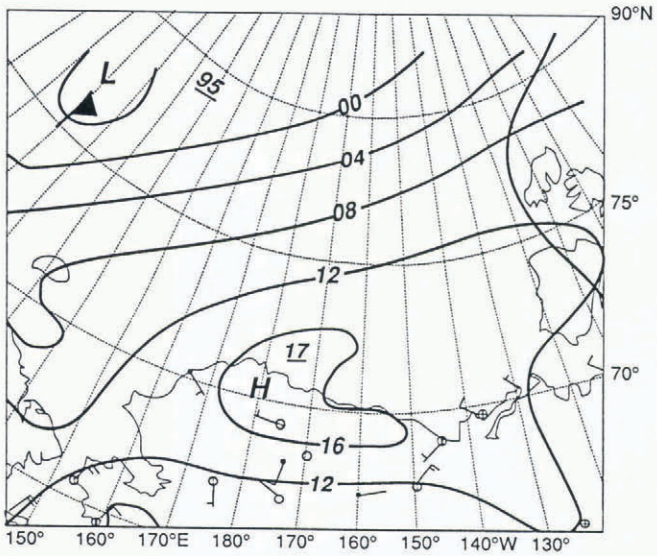

Fig. 2. Sea-level pressure map for 1800 h GMT, 6 April 1991. This pattern was typical of the flow regime over the Beaufort Sea during the period 31 March–6 April. Winds were generally southwesterly.

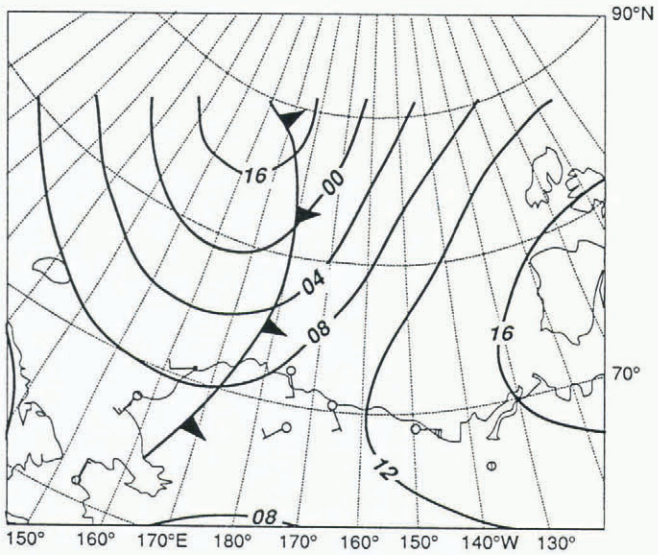

Fig. 3. Sea-level pressure map for 0000 h GMT, 8 April 1991 showing a strong frontal system across the Beaufort Sea. Prefrontal winds were from the south and post-frontal winds from the west creating a strong wind shear at the front.

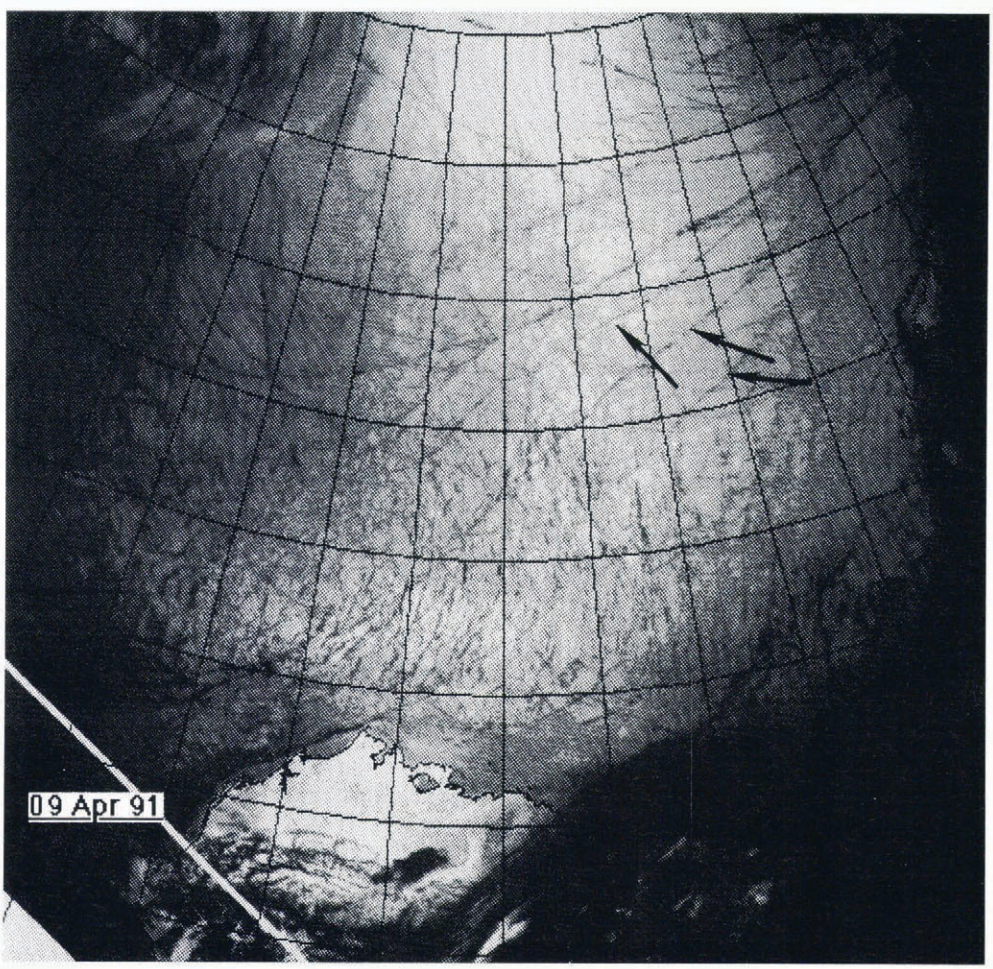

Fig. 4. AVHRR image (3 km resolution) for 1300 h GMT, 9 April 1991 showing changes that have occurred in the lead patterns since 1 April. Several more slip lines (arrows) can be seen to the south of the original long diagonal lead.

the front having a slightly more westerly than southwesterly component. Then on 7 April a strong cold front moved across the Beaufort Sea (Fig. 3) with strong southerly prefrontal winds and winds from the west behind the front. After this frontal passage several additional long leads appeared to the south of the original diagonal lead, positioned at an angle of about 30° to the original lead (Fig. 4). With westerly winds

https://doi.org/10.3189/S0260305500012878 Published online by Cambridge University Press

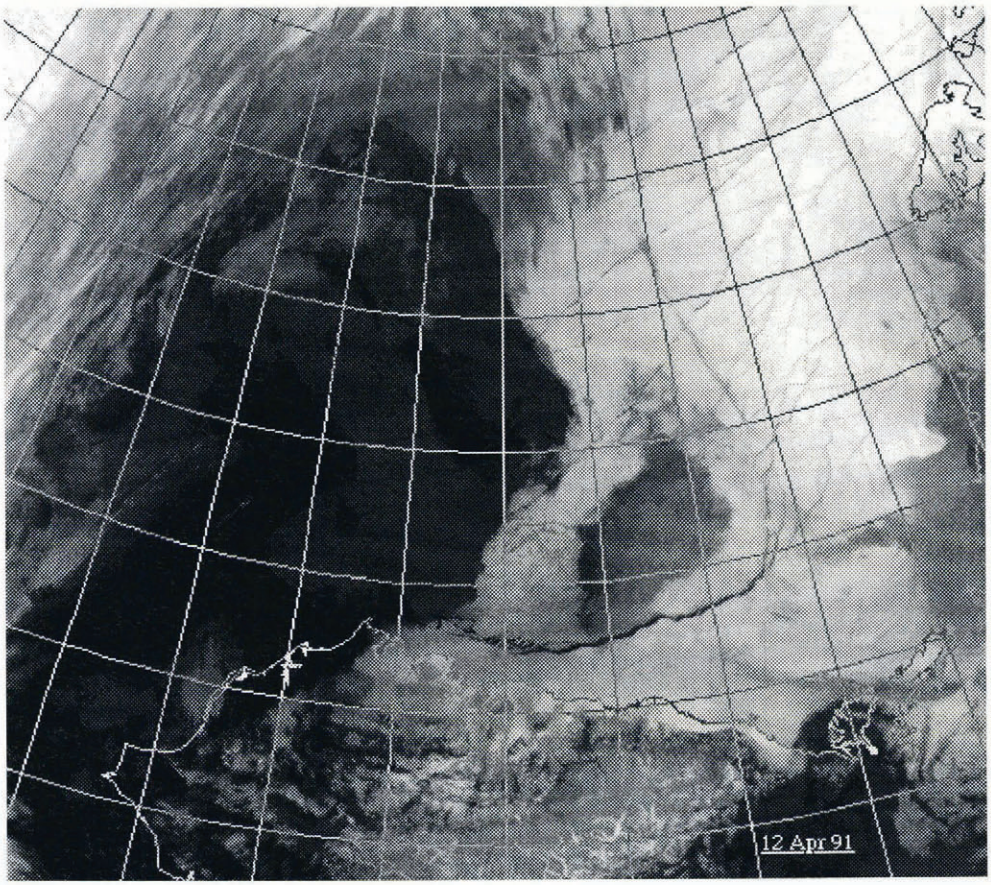

Fig. 5. AVHRR image (3 km resolution) for 1300 h GMT, 12 April 1991 showing the large coastal lead that has opened up along the north coast of Alaska due to the prolonged period of strong southerly winds over the Beaufort Sea.

behind the frontal system continuing on 8 and 9 April these new leads partially closed. We conjecture that the stresses induced by westerly winds prior to the passage of the frontal system were large enough to have exceeded the yield strength of the existing ice cover, giving rise to the lead system. Next there was divergence with southerly winds opening up the pattern followed by shearing deformation with westerly winds. From 10–14 April a low over the Chukchi Sea and a high over the southeastern Beaufort Sea resulted in an extended period of strong southerly winds during which these leads reopened and a large coastal lead formed along the Alaska coast (Fig. 5).

ICE VELOCITIES

In this section we analyze the lead motions and changes that took place in the lead patterns during the above meteorological regimes. Day-to-day lead motion images were generated on a Macintosh IIfx image-processing workstation by first inverting the look-up table (i.e. making a negative) of the first image. This image was then combined with the image for the following day using a logical AND operation. The result was an image in which the leads for the first day were white and the leads for the second day were black. Quantitative measurements of the lead motions could then be obtained from this composite image.

31 March–5 April

This time period continued a period of southwesterly winds over the Beaufort Sea. For the week prior to 31 March the Beaufort Sea was under the influence of very strong northwesterly to westerly winds which compacted the ice along the Alaskan coast and the eastern boundary of the Beaufort Sea formed by Banks Island and the Canadian Archipelago. As noted above, the result of this prolonged period of forcing of the ice with a wind having a westerly component was to shear off the northern part of the Beaufort Sea ice pack, creating a long lead oriented in a southwest to northeast direction diagonally across the Beaufort Sea (Fig. 1, arrow). This is the state of the ice pack at the start of the analysis of the AVHRR time series.

Figure 6 shows total lead displacements for the period 31 March to 5 April. The 31 March lead positions are shown by the white leads in the image and those for 5 April by the black leads. As can be seen, there was essentially no north–south movement of the diagonal lead during this period, and the lead motion to the north of the diagonal lead was parallel to this lead and in a northeasterly direction. Upon closer examination there is a second lead (arrow "B") parallel to the main diagonal lead (arrow "A") and located 120–140 km to the northwest. Relative movement across lead A during the time period was less (6–8 km or 0.016 m s^{-1}) than the combined relative movement across leads A and B (15–

https://doi.org/10.3189/S0260305500012878 Published online by Cambridge University Press

17 km or 0.037 m s^{-1}). Movement near the northwest corner of the image was as large as 22–25 km (or 0.052 m s^{-1}). Thus during this period of relatively uniform winds there was a velocity shear in the ice pack oriented northwest–southeast and concentrated at slip lines. The lead patterns translate intact as coherent units, where the coherence length is on the order of the large-scale diamond patterns (≈150 km). The pattern goes from that of shear deformation (Erlingson, 1988, fig. 6c) to non-cohesive opening and back to shear deformation.

5–9 April

During the period 5–9 April (Fig. 7), there was movement of the lead/slip line (lead A, Fig. 6) toward the northwest due to increased southerly winds. The slip line is now also a line of opening divergence. This main lead moved 5–6 km during the period and the distance moved was nearly the same along the line. Lead motion continued toward the northeast in the region to the north of the slip line; in this case though the relative motion with distance from the main slip line was the reverse of that for the period 31 March–5 April. Movement was 18–20 km just to the north of the slip line and 9–10 km farther to the north. The reversal of the shear direction was probably due to divergence in the ice field in the area near the slip line and convergence in the far field.

9–14 April

During the period 9–14 April persistent southerly winds continued to move the original slip line to the north and to open the large lead in the southern Beaufort along the Alaska coast (Fig. 5).

AN ARGUMENT FOR THE FRACTAL NATURE OF ICE

An interesting issue for sea ice is the near scale-invariant (or fractal) nature of the crack patterns seen in satellite imagery. Examples of this can be seen in Figure 8. The large-scale diamond-shaped patterns have a spacing of about 150 km and acute breaking angles of approximately 30°. The smaller-scale lead patterns have spacings of tens of km with similar breaking angles.

Consider the one-dimensional case of the sea-ice momentum balance in the x direction, with a frictional drag term dependent on the ice velocity, u_i, an external wind stress, τ_a, and the compressional stress σ,

Fig. 6. Lead motion composite image (1 km resolution) for the period 31 March–5 April 1991. White leads are for 31 March and black leads for 5 April 1991.

https://doi.org/10.3189/S0260305500012878 Published online by Cambridge University Press

Fig. 7. Lead motion composite image (1 km resolution) for the period 5–9 April 1991. White leads are for 5 April and black leads for 9 April 1991.

Fig. 8. AVHRR image (1 km resolution) for 1300 h GMT, 1 April 1991 showing that within the larger-scale (≈150 km) lead features are smaller-scale (≈10–20 km) lead structures of similar shape and with similar breaking angles (≈ 30°).

https://doi.org/10.3189/S0260305500012878 Published online by Cambridge University Press

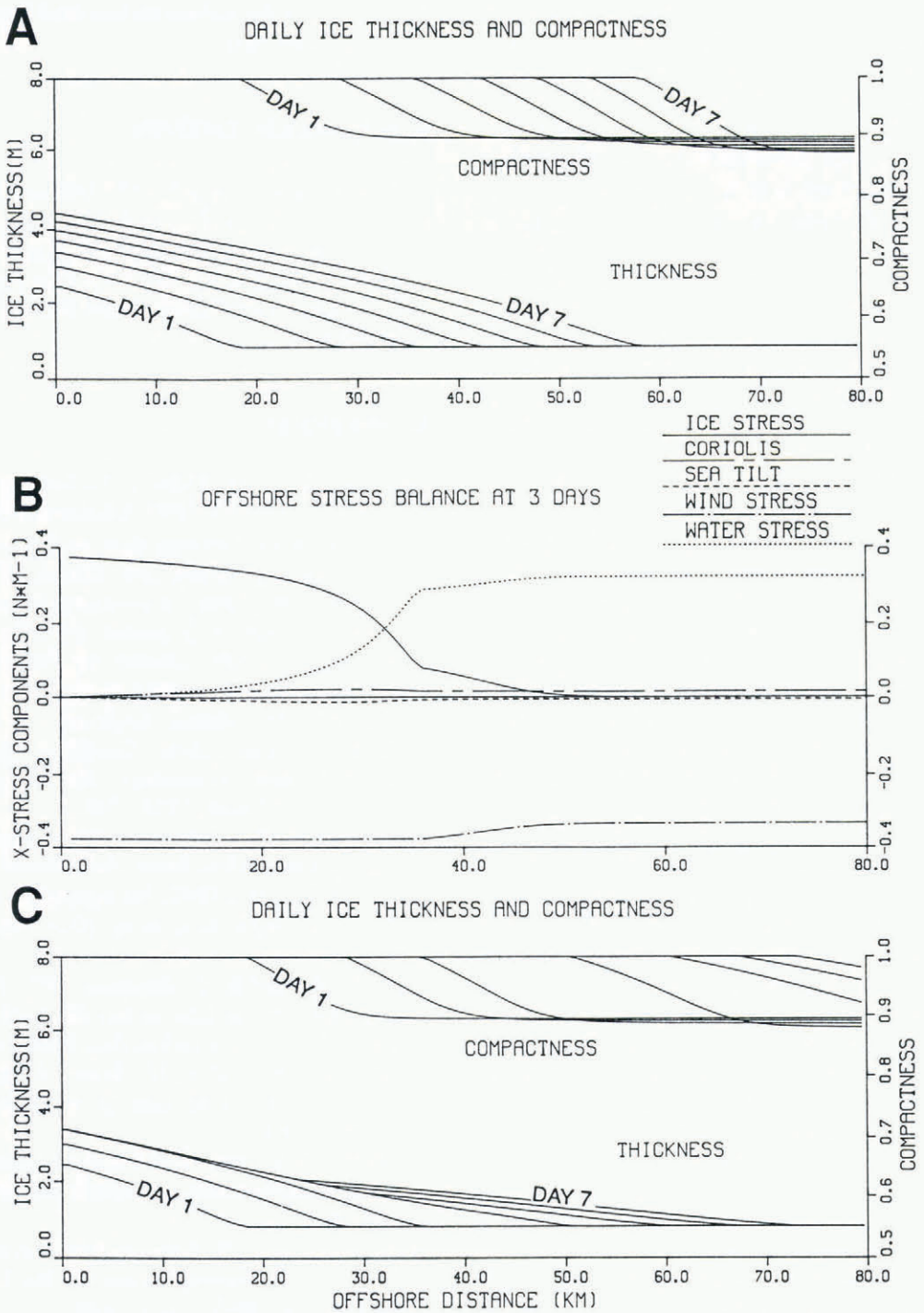

Fig. 9. (a) Results of a simulation for an onshore wind of 10 m s^{-1} and other standard parameters as in Overland and Pease (1988). The panel gives the daily ice compactness and thickness for day 1 through day 7. (b) The offshore stress balance shows a shift from a wind stress/water stress balance to a wind stress/internal ice-stress divergence balance near the point of 1.0 compactness. (c) Similar to Figure 9a except the wind speed was reduced from 10 m s^{-1} to 5 m s^{-1} from day 3 to day 4. Note that the ice does not continue to thicken in the nearshore zone (< 20 km) after the reduction in wind. In this region the ice strength gradient which developed to balance an onshore wind of 10 m s^{-1} is greater than the internal ice stress divergence necessary to balance a 5 m s^{-1} wind.

$$O = \tau_a + \frac{\partial \sigma}{\partial x} - cu_i \qquad (1)$$

We consider a hardening plastic rheology, that the y stresses are such that the one-dimensional case is valid and that there is a coastal wall at $x = 0$. A hardening plastic is one in which the strength can increase with state variables such as ice thickness. A one-dimensional case implies that there is a confining stress in the y direction such that its gradient is zero. Hibler (1986) investigated the case with a constant wind blowing toward shore and a uniform ice strength, P^*; all the deformation is at the coastline and integration of Equation (1) gives

$$\sigma(x) = -P^* + (cu_0 - \tau_a)x, \qquad \sigma < 0. \qquad (2)$$

For the offshore region the stress is below the yield criteria of $-P^*$.

https://doi.org/10.3189/S0260305500012878 Published online by Cambridge University Press

A second case is the solution for Equation (1) in which P^* is proportional to h^2 for a hardening plastic and quadratic dependence for friction (Overland and Pease, 1988); the ice thickness is h. Figure 9a shows the growth of the coastal rubble zone and a ridging front for their model after one through seven days for an onshore wind of $10\,\mathrm{ms}^{-1}$. The entire ice field landward of the ridging front is yielding with stress gradient based on the spatial gradient of ice strength balancing the wind stress (Fig. 9b). If the wind is reduced to $5\,\mathrm{m\,s}^{-1}$ after day 4 (Fig. 9c) the strength gradient in the nearshore region is greater than the wind stress and the ice will be motionless landward of 25 km. In the case of Hibler (1986) P^* is a constant with deformation only at the coastline $\sigma(x = 0) = -P^*$. In the second case we had $\partial\sigma/\partial x \sim$ constant with $\sigma \sim P^* \sim h^2$.

A way to look at the condition for the stress gradient remaining nearly constant is to consider the space scale over which the stress will vary. Large strength gradients can be maintained over large distances (hundreds of km) while on short length scales (~ 1 km), the yield criteria is quickly reached for modest values of strength. Thus we can build up a picture of an ice field composed of multiple scales. On the smallest deformation scale we have a stress gradient at the yield point where the absolute magnitude of the stress is small but the local gradient of stress is large. At larger scales, stress from the smaller interactions accumulates. Collectively, these regions require a larger ice stress to deform because of the greater horizontal distances involved. In certain strong ice strength regions, built from previous storms, the strength gradient is steeper than that required to balance the applied wind stress load; i.e. the icefield is below the yield point. Thus we have a fractal-like model where the ice is not ridged at one location as in the first case presented but is yielding on all length scales to form the composite picture (Fig. 8). That the distribution of the depth of ice keels per km follows a negative exponential (Wadhams and Davy, 1986), adds further support.

SUMMARY

By analyzing the motion of sea ice in the Beaufort Sea during a southwesterly to southerly wind regime we have been able to corroborate the theoretical results of Erlingsson concerning the breaking angles of ice forced by a wind field. We note that time-dependent winds can change a given icefield from being under shearing stress with leads at an acute angle to the wind direction to a non-cohesive opening pattern with the leads at 90° to the wind direction and then back to shearing. We have noted that a constant stress gradient can consist of a gradient of weaker (thinner) ice over short distances or stronger ice over greater distances. Both features must exist simultaneously to have the scale-invariant lead features seen in the 1–5 April 1991 case.

ACKNOWLEDGEMENTS

This research was supported by Office of Naval Research (ONR) contract N00014-91-C-0056 with Science Applications International Corporation (B.A.W.) and N00014-92-F-0013 with PMEL (J.E.O.). This paper is contribution No. 1365 from NOAA Pacific Marine Environmental Laboratory.

REFERENCES

Barry, R. G., M. W. Miles, R. C. Cianflone, G. Scharfen and R. C. Schnell. 1989. Characteristics of Arctic sea ice from remote-sensing data and their relationship to atmospheric processes. *Ann. Glaciol.*, **12**, 9–15.

Erlingsson, B. 1988. Two-dimensional deformation patterns in sea ice. *J. Glaciol.*, **34**(118), 301–308.

Erlingsson, B. 1989. Coastal sea ice deformations. *In* Axelsson, K. B. E. and L. A. Fransson, *eds. POAC 89. The 10th International Conference on Port and Ocean Engineering under Arctic Conditions, June 12–16 1989, Luleå, Sweden. Proceedings. Vol. 3.* Luleå, Tekniska Högskolan i Luleå, 1335–1347.

Erlingsson, B. 1991. The propagation of characteristics in sea-ice deformation fields. *Ann. Glaciol.*, **15**, 73–80.

Hibler, W. D., III. 1986. Ice dynamics. *In* Untersteiner, N., *ed. The geophysics of sea ice.* New York, Plenum Press, 577–640.

Marko, J. R. and R. E. Thomson. 1977. Rectilinear leads and internal motions in the ice pack of the western Arctic Ocean. *J. Geophys. Res.*, **82**(6), 979–987.

Overland, J. E. and C. H. Pease. 1988. Modeling ice dynamics of coastal seas. *J. Geophys. Res.*, **93**(C12), 15,619–15,637.

Pritchard, R. S. 1988. Mathematical characteristics of sea ice dynamics models. *J. Geophys. Res.*, **93**(C12), 15,609–15,618.

Sobczak, L. W. 1977. Ice movements in the Beaufort Sea 1973–1975: determination of ERTS imagery. *J. Geophys. Res.*, **82**(9), 1413–1418.

Steffen, K. 1987. Fractures in Arctic winter pack ice (North Water, northern Baffin Bay). *Ann. Glaciol.*, **9**, 211-214.

Wadhams, P. and T. Davy. 1986. On the spacing and draft distributions for pressure ridge keels. *J. Geophys. Res.*, **91**(C9), 10,697–10,708.

The accuracy of references in the text and in this list is the responsibility of the authors, to whom queries should be addressed.